

Sulfidation Impacts on the Hydrophobicity of Stepped Iron Surfaces

Jessica Jein White, Jack Jon Hinsch, Zhenzhen Wu, Yuhui Tian, William W. Bennett, and Yun Wang*

Nanoscale zero-valent iron (nZVI) has demonstrated high potential for the remediation of contaminated groundwater. Its lifetime is directly related to the hydrophobicity of nZVI. A promising approach to enhance the lifetime of nZVI is through sulfidation. Herein, the density functional theory (DFT) is applied to understand the impact of sulfidation on the hydrophobicity of stepped Fe surfaces. Adsorption properties of sulfur (S) at different coverages on the flat Fe(110) and stepped Fe(210) and Fe(211) surfaces are investigated. Sulfur has the stronger adsorption at a low surface coverage due to limited S–S repulsion. At the highest coverage ($\Theta = 1$ ML) on Fe(210) and Fe(211), the atoms at the step edges catalyze the formation of iron sulfides. The DFT results show surface hydrophobicity is mainly determined by the S coverage. At the low S coverage, the surface may become more hydrophilic due to the enhanced adsorption strength of water on the surface. However, an increase in the S coverage can efficiently block water adsorption, which is further evidenced by ab initio molecular dynamics (AIMD) results. The findings show that controlling S coverages is essential to engineer the hydrophobicity of nZVI surfaces for practical water remediation applications.

1. Introduction

Nanoscale zero-valent iron (nZVI) has great potential as a cost-effective and highly reactive material for groundwater remediation due to its large surface area and strong reductive capability.^[1–4]

J. J. White, J. J. Hinsch, Z. Wu, Y. Tian, Y. Wang
Centre for Catalysis and Clean Energy
School of Environment and Science
Griffith University
Gold Coast Campus, Southport, Queensland 4222, Australia
E-mail: yun.wang@griffith.edu.au

W. W. Bennett
Coastal and Marine Research Centre
Cities Research Institute
Griffith University
Gold Coast Campus, Southport, Queensland 4222, Australia

 The ORCID identification number(s) for the author(s) of this article can be found under <https://doi.org/10.1002/aesr.202300055>.

© 2023 The Authors. Advanced Energy and Sustainability Research published by Wiley-VCH GmbH. This is an open access article under the terms of the Creative Commons Attribution License, which permits use, distribution and reproduction in any medium, provided the original work is properly cited.

DOI: 10.1002/aesr.202300055

Its performance for specific contaminants is strongly related to surface hydrophobicity.^[3,5–10] However, nZVI has limitations regarding its reactive lifetime, contaminant selectivity, and mobility in subsurface environments, as water can easily oxidize nZVI through a side reaction of H₂ evolution.^[2,3,9,11–17] One solution to address this issue is the sulfidation of nZVI to form sulfidated nanoscale zero-valent iron (S-nZVI). In previous studies, S-nZVI has enhanced selectivity toward contaminants, improved reactivity, and extended the reaction lifetime.^[16,18–20] This is because the H₂ evolution side reaction can be suppressed by inhibiting the Fe/water interface.^[4,9,11,12,21–23] In addition, sulfidation can make the surface more hydrophobic,^[1,14,17] which favors the selective adsorption of hydrophobic contaminants, such as chlorinated organic compounds.^[20,24] The addition of sulfur to the Fe surface also increases charge redistribution, leading to a more reactive surface with a small bandgap

that facilitates efficient electron transfer from the Fe core to the surface of the particles.^[1,3,9,12,21] In contrast, when nZVI is oxidized, the bandgap increases, resulting in less efficient electron transfer.^[12]

Two methods can be used to produce S-nZVI: the one-step cosulfidation method and the two-step postsulfidation method.^[3,11,19] In the one-step cosulfidation method, dissolved iron is reduced by sulfur species (such as Na₂S or Na₂S₂O₄), forming S-nZVI. In contrast, the two-step postsulfidation method involves first synthesizing nZVI and then sulfidation is carried out. The main difference between these two methods is that the one-step method forms sulfur species in the Fe⁰ core and, to a lesser extent, throughout the surface layer of the S-nZVI particles.^[11,12] In contrast, the two-step method of producing S-nZVI involves sulfidation of presynthesized nZVI. The core Fe⁰ structure remains unchanged, indicating that sulfur is only adsorbed onto the surface of the particles.^[11,12,25] Numerous studies have been carried out to investigate the distinctions and resemblances between one-step and two-step S-nZVI production methods. One of the primary differences between these methods is related to hydrophobicity. One-step synthesized S-nZVI has a higher ratio of sulfur, which results in a hydrophobic surface.^[4] In contrast, the two-step method produces S-nZVI with a more hydrophilic in comparison with the one-step S-nZVI surface shown by the measured water contact angle.^[4] This difference in hydrophobicity

has implications for the reactivity of S-nZVI toward hydrophilic and hydrophobic contaminants, as well as the reactive lifetime of the particles. Thus, the coverage of sulfur on the Fe surface is critical depending on the target contaminant.^[4,5,24,26]

The density functional theory (DFT) simulations have been used in a number of studies to reveal the atomic properties of S-nZVI. Cao et al. undertook a DFT study to investigate the effect of sulfur on the Fe(110) surface.^[9] Studies have shown that when sulfur is adsorbed onto Fe(110), it leads to a more hydrophobic surface, which is indicated by an increase in the distance between the surface and water molecules. The presence of surface sulfur atoms blocks the adsorption sites of hydrogen atoms in water, slowing down the H₂ evolution side reaction. In a study by Xu et al.,^[17] computational methods were used to investigate water and hydrogen adsorption on pyrite (FeS₂) and mackinawite (FeS) surfaces and compare them with experimental results. They found that the pyrite surface was more hydrophobic due to the higher ratio of sulfur on the surface. On both surfaces, hydrogen was unable to be adsorbed onto the sulfur atoms and instead migrated from the S atom to the Fe atoms. This finding supports the idea that sulfur has a hydrophobic effect, which affects water adsorption and can also sterically hinder hydrogen adsorption on the Fe surface. Cao et al. employed DFT calculations to investigate the effect of sulfur on and in the Fe(110) surface.^[11] In their study, S-in-Fe(110) represents the “one-step” S-nZVI, where sulfur is incorporated into the Fe bulk structure, whereas S-on-Fe(110) represents the “two-step” S-nZVI, where sulfur is only adsorbed onto the surface without affecting the Fe bulk. The Fe(110) surface was highly hydrophilic, with water molecules adsorbing very favorably onto the Fe surface. However, both S-in-Fe(110) and S-on-Fe(110) were found to be hydrophobic. S-in-Fe(110) was observed to block the highest number of hydrogen adsorption sites, mainly due to its effect on the Fe surface atoms. In contrast, S-on-Fe(110) blocked fewer hydrogen adsorption sites, acting mainly as steric hindrance.

In our previous research, we discovered that stepped surfaces can significantly influence water adsorption and dissociation processes.^[27–29] Specifically, we used Fe(210) and Fe(211) as model systems and found that stepped surfaces are more reactive and more susceptible to corrosion by water than flat Fe(110).^[27,28] However, our current understanding of S-covered stepped nZVI surfaces are limited. To address this knowledge gap, we conducted DFT simulations with van der Waals correction to investigate S-doped Fe(211), and Fe(210) surfaces with either high or low S coverage. Our findings indicate that stepped nZVI surfaces are more readily sulfidized at high S coverage ($\Theta = 1$ ML). Moreover, high sulfur coverage changes the hydrophilic Fe surfaces to a hydrophobic one.

2. Computational Details

All DFT computations were performed using the Vienna Ab initio Simulation Package (VASP) based on the projector augmented wave (PAW) method with consideration of spin polarization.^[30,31] *Vaspkit* was used to build atomic models and postprocess the data.^[32] The optPBE exchange-correlation energy was employed with the consideration of vdW interaction correction.^[33–36] OptPBE was chosen as the method of choice

as it has shown in our previous papers to accurately represent Fe. The electron–ion interaction was described using the PAW pseudopotentials, with the 3s²3p⁶3d⁷4s¹, 2s²2p⁴, 1s¹, and 3s²3p⁴ treated as valence electrons of Fe, O, H, and S, respectively.^[37] A plane-wave basis set with a cut-off kinetic energy of 520 eV was used. The gamma-centered *k*-point meshes with a reciprocal space resolution of $2\pi \times 0.04 \text{ \AA}^{-1}$ and $2\pi \times 0.02 \text{ \AA}^{-1}$ were utilized for structural optimization and static self-consistent calculations, respectively. The convergence criteria for the self-consistent electronic and structural optimization loop were set to 1×10^{-5} eV and 1×10^{-3} eV \AA^{-1} , respectively.

The (110), (211), and (210) surfaces were modeled using the slab models, separated by a vacuum region of 15 Å to avoid interaction between the surfaces of neighboring slabs along the *z*-direction. The interlayer distance determined the choice for the number of atomic layers. The (210) surface has the smallest interlayer distance of $a_0/\sqrt{20}$, where a_0 is the lattice constant. As such, 21 atomic layers were used here. The (211) surface has a slightly larger interlayer distance with $a_0/\sqrt{6}$, hence 13 atomic layers were used. As a comparison, the interlayer distance of the (110) surface is $a_0/\sqrt{2}$. Thus, only seven atomic layers were used as previous studies have demonstrated that calculated surface properties could be converged when the layer number is higher than five.^[38] When the surface structures were optimized, the bottom 3, 5, and 7 layers were fixed at the bulk position for the (110), (211), and (210) surfaces, respectively. The positions of the atoms in the other topmost layers and the adsorbates were allowed to relax.

The adsorption energy for sulfur (ΔE_S) and molecular water (ΔE_{H_2O}) was calculated using the formulas:

$$\Delta E_S = \frac{1}{N} (E_{\text{Fe/S}_{\text{surf}}} - E_{\text{Fe}_{\text{surf}}} - NE_S) \quad (1)$$

$$\Delta E_{H_2O} = \frac{1}{N} (E_{\text{ad}_{H_2O}} - E_{\text{surf}} - NE_{H_2O}) \quad (2)$$

where N is the number of adsorbate molecules per unit cell. $E_{\text{Fe}_{\text{surf}}}$, E_{surf} , and $E_{\text{ad}_{H_2O}}$ are the energies of the intrinsic Fe surface, the Fe surface with or without the adsorbed sulfur, and the surface with adsorbed water, respectively.

In the ab initio molecular dynamics (AIMD) simulations, the $(1 \times 1 \times 1)$ gamma-centered *k*-point mesh was applied with a (2×2) supercell. To build the initial configuration of the AIMD calculations, PACKMOL in Winmostar was used.^[39] The canonical ensemble (NVT) was used with the Andersen thermostat to simulate the dynamic behavior of the water molecules at 350 K. The simulations were run for 4 ps with a step of 1 fs applied. The Fe–O radial distribution function (RDF) was calculated based on the distance between the oxygen in water and the iron surfaces.

3. Results and Discussion

3.1. Sulfur-Doped Fe Surfaces

First, different sulfur (S) adsorption sites were investigated on Fe(110), Fe(210), and Fe(211). Various S coverages (θ) were considered on each surface to determine the coverage effect on their

adsorption properties. The coverage is defined as the ratio between adsorbed S and the topmost surface Fe atoms in each surface cell. For Fe(110) and Fe(211), the coverages of 1, 1/2, and 1/8 ML were investigated. While on Fe(210), four different coverages at 1, 2/3, 1/3, and 1/12 ML were considered. All the adsorption sites investigated along with the coverages, adsorption energy, and bond length are listed in Table S1–S3, Supporting Information.

Figure 1 shows the stable adsorption configuration of S on Fe(110) at the different coverages. At the lowest coverage 1/8 ML, our DFT results reveal that the fourfold hollow site is the energetically preferred adsorption site, which is consistent with data reported by Spencer et al.^[40] There are two short Fe–S bonds with a length of 2.19 Å, which is almost identical to the reported Fe–S bond length at the GGA level.^[40] And two long Fe–S bonds with a length of 2.50 Å. When the coverage increases from 1/8 to 1/2 ML, the S–S bond length decreases from 5.66 Å to 2.83 Å when S adsorbs at the 4fh sites, which leads to the weakened adsorption energy of S atoms. Consequently, the S atoms prefer to adsorb at the threefold hollow (3fh) sites with longer S–S distances, while the coordination number of S in terms of Fe changes from 4 to 3. This indicates that the S–S repulsion can greatly affect the adsorption strength of S on Fe(110) surfaces. This is further demonstrated by the weaker adsorption strength when the S coverage increases to 1 ML. The adsorption energy is only about 2/3 of that when the coverage is 1/8 ML due to the shorter S–S distance and strong S–S repulsion. Accordingly, the shortest S–Fe bond length also increases from 2.19 to 2.34 Å at the coverage of 1 ML.

On the Fe(211) surface, a similar trend was observed (see **Figure 2**). At the lower coverage of 1/8 ML, S atoms prefer to adsorb at the fourfold hollow (4fh) site to maximize the coordination number to the surface Fe atoms. When the coverage increases to 1/2 ML, the threefold hollow (3fh) is energetically preferred to minimize the S–S repulsion. Different from S adsorption on Fe(110) at the coverage of 1 ML, half of the S atoms are 3.87 Å higher than the topmost layer of the surface on the Fe(211) surface. The rest of the S atoms adsorb at the 4fh site. The strong S–S repulsion can be ascribed to the smaller S–S distance on Fe(211). At the coverage of 1 ML, the S–S distance along

the y direction is 2.45 Å on Fe(211), which is 16% shorter than on Fe(110). Interestingly, the S adsorption strength on Fe(211) is slightly weaker than that on Fe(110) when the S coverage is low. However, the S atoms more tightly interact with the Fe(211) surface at the coverage of 1 ML, which may be due to the reduced S–S repulsion by elevating half of the S atoms above the surface. Again, the adsorption properties on Fe(211) confirm the importance of S–S repulsion at high coverage.

Four sulfur coverages were investigated on the Fe(210) surface at 1, 2/3, 1/3, and 1/12 ML. The most stable adsorption configurations are shown (see **Figure 3**). At the low coverage of 1/12 ML, the most stable adsorption site is a sixfold hollow (6fh) site at the edge. When the S coverage increases to 1/3 and 2/3 ML, S atoms adsorb onto both 6fh and 3fh sites. At the highest coverage of 1 ML, S atoms adsorb on 6fh, 3fh, and a top bridge site. These sites are associated with the surface Fe atoms with the lowest coordination number of 4 (CN4) at the edge. Consequently, the CN4 Fe atoms in the stepped (210) surface dissociate from the rest of the surface atoms, which may further cause the formation of surface sulfides, e.g., FeS and FeS₂, as observed in experiments.^[8,11] Our DFT results, therefore, suggest that the sulfidation of nZVI may start at the stepped facets of nanoparticles. These findings also support the occurrence of iron dissolution during the formation of iron sulfides. This is consistent with previous experimental observations that suggest the initial dissolution of iron during iron sulfide formation.^[9] Additionally, it agrees with a separate investigation that highlights the increased iron dissolution observed when comparing S-nZVI to pristine nZVI.^[41] The iron dissolution can be ascribed to the Kirkendall effect, where outward diffusion of iron is faster than the inward diffusion of sulfur. This phenomenon leads to the formation of hollow structures under conditions of high sulfur content and prolonged sulfidation time.^[25] However, the theoretical understanding of the Kirkendall effect is beyond the scope of this study and will be the subject of future investigations.

At higher coverage, the adsorption energies increase on all Fe surfaces, which means weakened adsorption, as sulfur adsorption depends on the distance between the sulfur atoms. The larger S–S distance may strengthen the adsorption of S

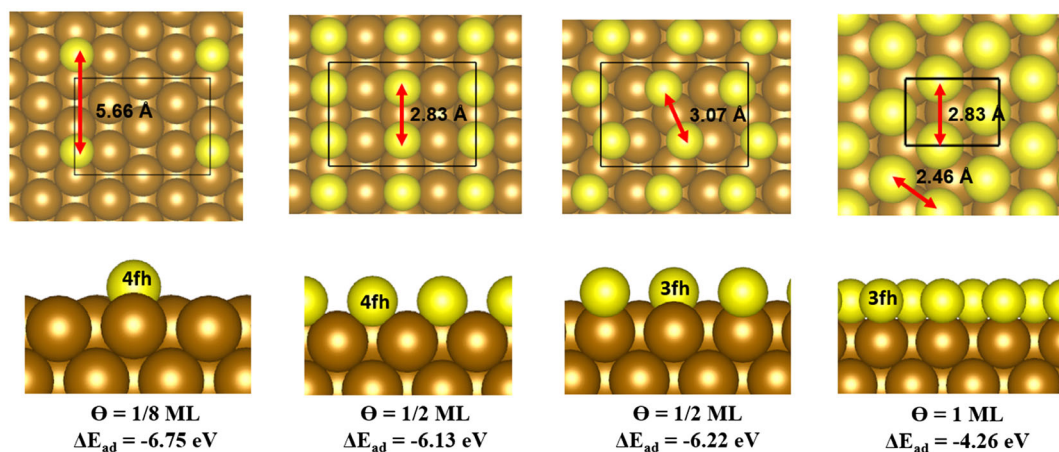


Figure 1. The top (up) and side (down) views of the most stable atomic configurations of Fe(110) surface with adsorbed S atoms at different coverages with the distances between adsorbed S atoms (brown = Fe, yellow = S).

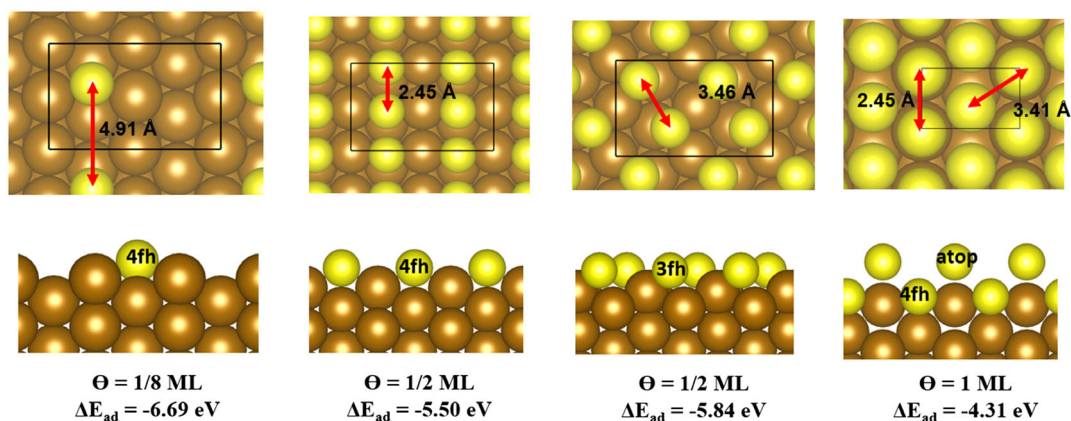


Figure 2. The top (up) and side (down) views of the most stable atomic configurations of Fe(211) surface with adsorbed S atoms at different coverages with the distances between adsorbed S atoms (brown = Fe, yellow = S).

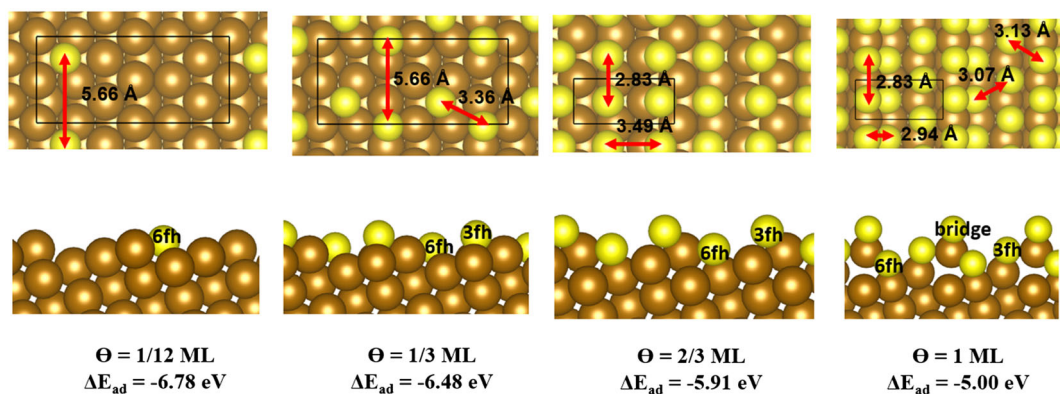


Figure 3. The top (up) and side (down) views of the most stable atomic configurations of Fe(210) surface with adsorbed S atoms at different coverages with the distances between adsorbed S atoms (brown = Fe, yellow = S).

atoms, as evidenced by the S adsorption on (110) and (211) surfaces at the coverage of 1/2 ML. This demonstrates that the S–S repulsion has a high impact on the adsorption properties of S. According to our previous research, the strength of oxygen atom adsorption on the Fe surface is dependent on the number of associated Fe atoms, the coordination number of surface Fe atoms, and Fe–O bond length. Conversely, these factors have little impact on adsorption strength at low S coverage. Specifically, the adsorption energies for S on all three surfaces are comparable, with a minimal difference of 0.1 eV, while for oxygen, the difference is greater than 0.5 eV. This disparity could be attributed to the weaker interaction between S and the surfaces. The partial crystal orbital Hamilton population ($-p\text{COHP}$) analysis was conducted at the most favorable adsorption sites on the three Fe surfaces at the lowest coverage to understand the bonding mechanism between the atomic sulfur and the associated Fe atoms. The bonding and antibonding mechanisms can be characterized based on the positive and negative overlap populations. The covalent bond strengths between Fe and S atoms are quantitatively determined by taking the integral of $-p\text{COHP}$ ($-I_p\text{COHP}$) up to the Fermi level. The trend follows (110) > (211) > (210), which is further supported by the partial density of states (pDOS) shown in **Figure 4**. The covalent

bonding can be related to the hybridization between the Fe 3d states and S 4p states at the bonding energy range from -6 to -4 eV. On the (110) surface, the hybridization between states is the strongest, as suggested by the largest overlap. Such hybridization is weakest on the (210) surface, which matches the COHP conclusion. This covalent bonding strength trend is the same as the corresponding S–Fe bond lengths, which are 2.17, 2.30, and 2.36 Å on the (110), (211), and (210) surfaces, respectively. This trend is different from the COHP analysis result between O and surface Fe atoms, which follows (211) > (210) > (110).^[28] This may be ascribed to the strong covalent S–Fe bonding characteristics. As a result, the bond length becomes the dominant factor in determining the covalent bonding strength, as suggested by the $-I_p\text{COHP}$ values and pDOS patterns.

3.2. Water Adsorption on Sulfur-Doped Fe Surfaces

Our previous study demonstrated that nZVI is hydrophilic and water adsorption and dissociation processes occur spontaneously.^[27] The surface atoms mainly catalyze the water dissociation with low CNs at stepped Fe(210) and Fe(211) surfaces. To explore the sulfidation impacts on the hydrophobicity of nZVI,

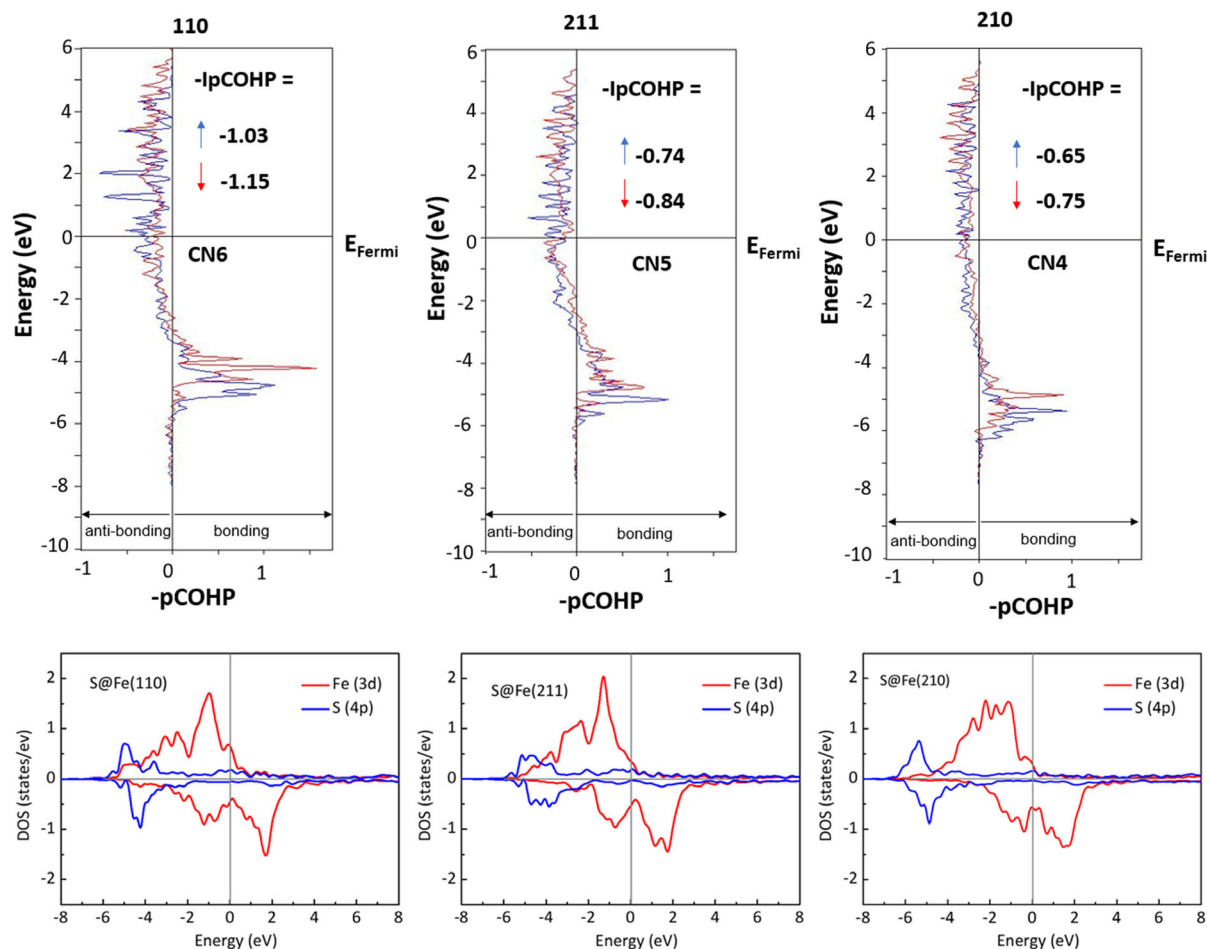


Figure 4. Partial crystal Hamiltonian population ($-p\text{COHP}$) analysis between the bond of the adsorbed sulfur atom and the surface with the lowest CN at the most favorable adsorption site of three Fe surfaces. The bonding and antibonding states are positive and negative, respectively. The upward and downward arrows indicate spin up and down states, respectively.

we conducted a comprehensive investigation to examine the effect of adsorbed S atoms on the highly reactive steps of Fe(210) and Fe(211) compared to the thermodynamically stable Fe(110) surface (Table S4 and S5, Supporting Information).

Two sulfur coverages at 1/8 and 1/2 ML were considered for molecular water adsorption on the Fe(110) surface. On the 1/8 ML coverage, the water was found to be -0.45 eV, which is similar to the pristine Fe(110) surface with adsorption energies of -0.43 and -0.47 eV. In contrast, it was found that the water adsorption was very weak at 1/2 ML coverage when water is adsorbed near the S. This is because the Fe–O interaction was significantly weakened, as evidenced by Fe–O bond distance of 4.65 Å at an S coverage of 1/2 ML. For comparison, the bond distance between Fe–O on the pristine Fe(110) surface was 2.25 and 2.77 Å at the water coverage of 1/8 and 1/2 ML. This suggests that an increase in the adsorption of S atoms on the Fe(110) surface can effectively reduce hydrophilicity. At 1/2 ML S adsorption, the adsorption strength of molecular water is mainly due to hydrogen bonding between H atoms and adsorbed S atoms, as shown in Figure 5. The H–S bond lengths. Our results agree with the reported results of Li et al. and Cao et al. that sulfur

adsorption on the Fe(110) surface can lead to a more hydrophobic Fe(110) surface.^[11,42]

On the (211) surface, two sulfur coverages at 1/8 and 1/2 ML were investigated for molecular water adsorption (see Figure 6). On the pristine Fe(211) surface, the water adsorption energy is -0.60 eV. At the low sulfur coverage of 1/8 ML on the (211) surface, the water adsorption is more favorable with -0.66 eV. The enhanced water adsorption strength can be ascribed to the synergetic interactions between water and the S-doped Fe(211) surface. The O in H_2O can still interact with active surface Fe atoms with a low coordination number on the pristine surface. In contrast, the H atom in water can form a hydrogen bond with S atoms, as evidenced by the short H–S distance of 3.13 Å. Such strong water adsorption was not observed on the S-doped Fe(110) surface. This may be ascribed to the flat Fe(110) surface without active surface atoms with low coordination numbers and specific stepped configurations. When the S coverage increases to 1/2 ML, all the active surface Fe atoms have been effectively blocked by the S atoms. Consequently, the shortest distance between the O atom in water to surface Fe atoms increases to 4.48 Å. Similar to that on the S-doped Fe(110), the adsorption

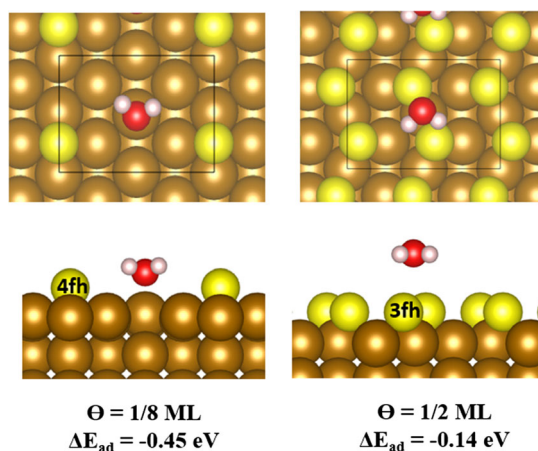


Figure 5. The top (up) and side (down) views of the most stable water adsorption atomic configurations on S–Fe(110) (brown = Fe, yellow = S, red = O, white = H).

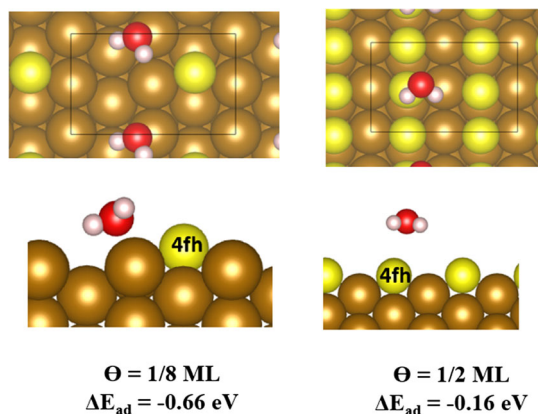


Figure 6. The top (up) and side (down) views of the most stable atomic configurations of S–Fe(211) surface (brown = Fe, yellow = S, red = O, white = H).

of molecular water is mainly through S–H bonding. The shortest S–H bond length is 3.15 Å. As a result, the adsorption energy of

molecular water on the S-doped (211) surface is -0.16 eV at the S coverage of $1/2 \text{ ML}$, which is almost identical to that on the S-doped (110) surface.

The adsorption properties of molecular water on the Fe(210) surface were investigated at three different coverages ($1/12$, $1/3$, and $2/3 \text{ ML}$). **Figure 7** shows the most stable adsorption configurations at different coverages. At $1/12$ and $1/3 \text{ ML}$ sulfur coverages, the water adsorption energies are -0.68 and -0.77 eV , respectively, which are even lower than that of molecular water adsorption on the pristine Fe(210) surface of -0.63 eV . This is because the O atom in water can still interact with the surface Fe atoms. The shortest Fe–O bond lengths are 2.51 and 2.74 Å at a coverage of $1/12$ and $1/3 \text{ ML}$, respectively. At the same time, the H atoms in water can form bonds with the surface S atoms when the coverage of water is low. The shortest S–H bond lengths are 2.57 and 2.01 Å at $1/12$ and $1/3 \text{ ML}$ coverage, respectively. At $1/3 \text{ ML}$ coverage, both hydrogens on the water molecule interact with the preadsorbed sulfur atoms, resulting in even more favorable adsorption. The Fe–O distance was 2.21 Å at $1/12$ coverage and 3.07 Å at $1/3 \text{ ML}$ coverage. A higher S coverage of $2/3 \text{ ML}$ was investigated on the Fe(210) surface to assess its impact on the water and Fe interaction. It was found that at this higher coverage, the adsorption was weaker (-0.25 eV), with the Fe–O distance increasing to 3.78 Å. All the considered sites, coverage, adsorption energy, and bond lengths can be found in Table S4 and S5, Supporting Information.

In summary, our DFT results demonstrate that a low S coverage on the stepped surface has a minor impact on hydrophobicity. The existence of S–H bonding can even increase the hydrophilicity of the stepped surface. However, when the S coverage increases moderately to $1/2$ and $2/3 \text{ ML}$ on Fe(211) and Fe(210), respectively, water adsorption on the surface can be greatly weakened. As a result, the stepped surface can become hydrophobic at relatively high S coverages. S–nZVI is a special material that can incorporate sulfur either into the bulk of the iron or exclusively on the surface. Two methods, namely cosulfidation, and postsulfidation, are commonly employed for this purpose.^[6,11,42] In the cosulfidation method, sulfur reacts with the ZVI core, resulting in the formation of iron sulfides, such as mackinawite and pyrite.^[11,17] In contrast, the postsulfidation method involves the adsorption of sulfur exclusively onto the surface of the pristine nZVI.^[11,25] In our study, we specifically

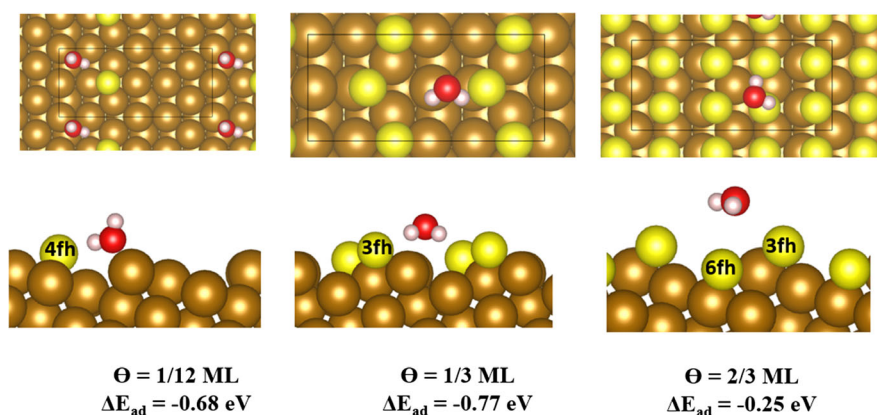


Figure 7. The top (up) and side (down) views of the most stable molecular water adsorption on S–Fe(210) (brown = Fe, yellow = S, red = O, white = H).

focused on the postsulfidation S-nZVI variant, where sulfur is solely present on the surface. The cosulfidation method, as investigated by Kolos et al.,^[2] involves the formation of iron sulfides within the nZVI, resulting in materials such as mackinawite and pyrite. Their findings align with our research. Both studies revealed that the introduction of sulfur does not necessarily increase the hydrophobicity of the surface. Our study demonstrated that only a high coverage of sulfur resulted in weaker adsorption. This is consistent with their observations regarding mackinawite, where water is repelled, and hydrogen and sulfur bonds are formed. In the case of pyrite, their study observed stronger water adsorption compared to the plain Fe(111) surface, primarily due to the bonding between oxygen and Fe, as well as hydrogen and sulfur interactions. Interestingly, the higher sulfur content in pyrite led to stronger adsorption, indicating that the structure of sulfides also plays a subtle role in determining hydrophobicity.

3.3. Water Adsorption on Clean and Sulfur-Doped Fe Surfaces using Ab Initio Molecular Dynamics

Since the above DFT studies largely ignore the interaction between the water molecules, these results can only be used to understand the adsorption properties of individual water molecules on S-doped Fe surfaces. To better understand the Fe/water interface, atomic models of the interface with the explicit water molecules on the surfaces were built. AIMD calculations were completed for both the pristine Fe surfaces and the sulfur-doped surfaces at S coverages of 1/2 ML on Fe(110) and (211). On the Fe(210) surface, both 1/3 and 2/3 ML coverages were considered. The snapshot structures during AIMD are shown in **Figure 8**. To quantify the hydrophobicity of each surface, the radial distribution function (RDF) was investigated to measure the water molecule placement toward the Fe surfaces (**Figure 9**).

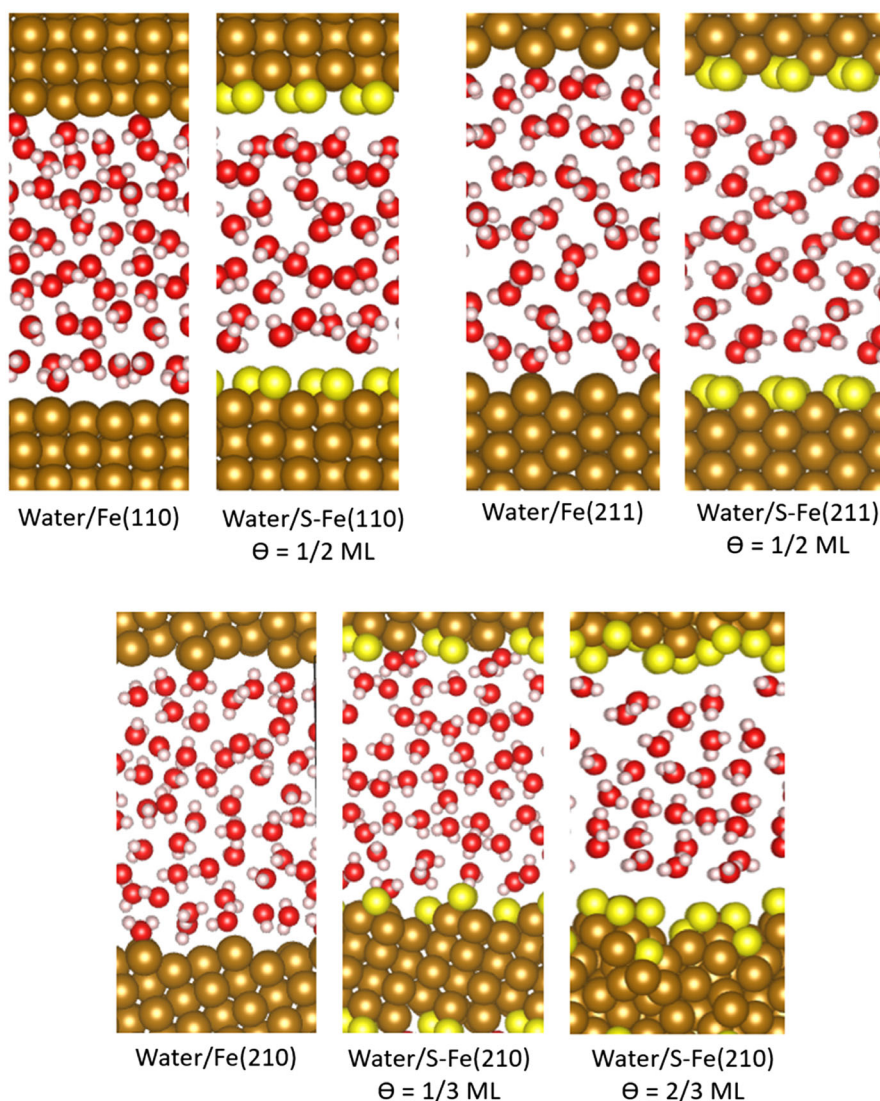


Figure 8. Screenshots of the atomic structures of Fe/water interface without or with adsorbed S atoms at the specific ML coverage (Θ) after 4-ps AIMD simulations.

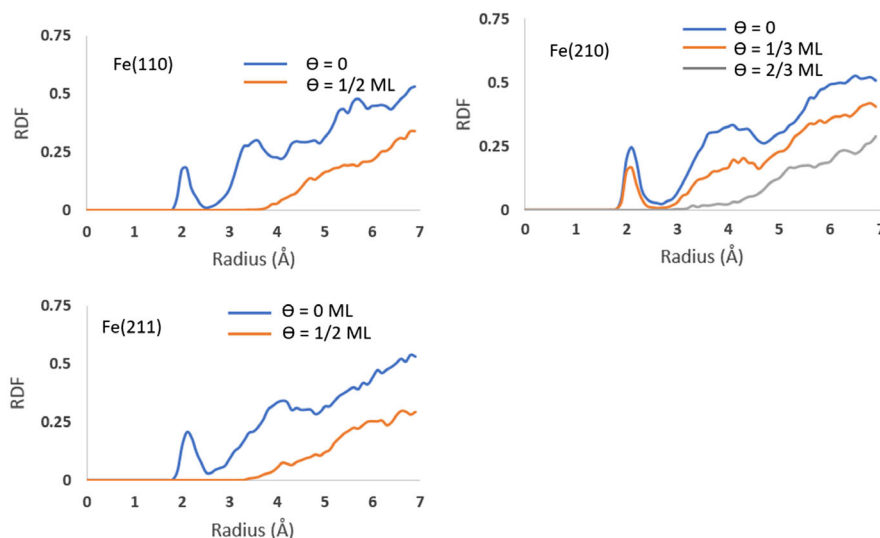


Figure 9. Radial distribution function (RDF) between the oxygen in the water molecule and the surface Fe atoms at different sulfur ML coverage (Θ).

On the pristine surfaces, Fe–O bonds have been formed during the simulation, as shown in Figure 8. It is noted that the O in water mainly interacts with the surface Fe with the lowest CN on the stepped (211) and (210) surfaces. Again, this matches our previous study showing that surface Fe atoms with low CN are active for molecular water adsorption. After the sulfidation at 1/2 ML S coverage, there are almost no Fe–O bonds formed on the Fe(110) and Fe(211) surfaces, which suggests that the surface changed from hydrophilic to hydrophobic—this is consistent with the DFT results on the molecular water adsorption properties. On the Fe(210) surface, we can still observe Fe–O bonding at 1/3 ML coverage, which suggests that the S coverage is still too low to completely block water adsorption on this stepped surface. However, unlike single molecular water adsorption, there is no bonding between S and H in the adsorbed water molecules. In contrast, the H atoms in the adsorbed water can form hydrogen bonds with O atoms in other water molecules. This can be understood because H–O hydrogen bonding is stronger than the S–H bond. Additionally, the S–H bonding is the main contribution to the molecular adsorption on the three S-doped Fe surfaces at high S coverage in our DFT results. As a result, water adsorption can be further weakened due to the stronger O–H hydrogen bonding in the water solution as shown by the AIMD simulations. It was found that the high sulfur coverage on Fe(210) surface led to the breakdown of the Fe surface due to the migration of the sulfur into the Fe bulk. This is because at a high coverage sulfur atoms form strong bonds with the Fe atoms in the surface. This can cause a surface reconstruction leading to changes in the arrangement and stability of the surface atoms.

The Fe–O RDF analysis further supports the impact of sulfidation on the hydrophobicity of three Fe surfaces. As shown in Figure 9, there is a peak at 2.1 Å on the three pristine Fe surfaces. This peak can be ascribed to the molecularly adsorbed water on the surface with relatively short Fe–O bonds. After the sulfidation at a relatively high S coverage (1/2 ML on Fe(110) and Fe(211), 2/3 ML on Fe(210)), this peak disappears. Interestingly, the peak around 2 Å still has a much lower height

on the Fe(210) surface when the S coverage is 1/3 ML. This confirms that the surfaces become more hydrophobic after sulfidation, even though the single water molecule on the S-doped surface may have stronger adsorption. Such subtle differences can be explained by the existence of relatively strong hydrogen bonding between water molecules in the liquid phase. Based on the AIMD results, the water adsorption can be efficiently blocked by sulfidation, which could significantly improve the lifetime of nZVI. Our AIMD results also demonstrate that sulfidized Fe surfaces' hydrophobicity is linked to the S coverage. This S coverage-dependent behavior matches reported experimental observations. The one-step synthesized S-nZVI has a higher S coverage, which results in a hydrophobic surface.^[4] In contrast, the S-nZVI from the two-step method produces a hydrophilic surface because the sulfur is only present on the surface and not incorporated into the particles. The agreement between theoretical and experimental results suggests the consideration of steps in nZVI is essential to provide a holistic understanding of the impact of sulfidation on the hydrophobicity of nZVI particles. It is worth noting that The Fe–O PDF patterns of the Fe(210)/water and S-doped Fe(210)/water interfaces obtained using a denser ($2 \times 2 \times 1$) k -point mesh exhibit remarkable similarity to those obtained using the ($1 \times 1 \times 1$) k -point mesh, as shown in Figure S1, Supporting Information. This suggests that the gamma-only k -point mesh used in the AIMD analysis of this study is sufficient.

4. Conclusion

This study investigated the addition of sulfur on stepped nZVI surfaces to weaken the molecular water and Fe interaction. It was found that the addition of sulfur can weaken the interaction at both low and high coverages. At all surfaces at low coverages, the water molecule was able to have a weak interaction above the sulfur atom and a stronger interaction above the uncovered Fe atom. At high coverages, however, Fe(110) and Fe(211) had weak molecular water adsorption from any angle. However, at

1/3 ML coverage on the Fe(210) surface, due to uncovered Fe atoms, strong molecular water adsorption was able to occur (coverage needed to increase to 2/3 ML to prevent this interaction). AIMD calculations were also conducted to investigate the impact of water liquid (in comparison to just one for the DFT calculations). It was found that the surface became even more hydrophobic with the consideration of a greater number of water molecules as the water molecules formed O–H bonds between themselves instead of forming S–H bonds. This study demonstrates that the ratio of sulfur is important and changes the properties of the nZVI surface. Our results support the experimental studies that a higher ratio of sulfur leads to a more hydrophobic surface. Our results also reveal that the addition of sulfur at the low S coverage can lead to more favorable water adsorption dependent on the water molecule angle due to the formation of the hydrogen and sulfur bonding as well as the Fe and oxygen interaction. Further studies can use these results to investigate the best sulfur coverage on nZVI for targeting the remediation of hydrophobic and hydrophilic contaminants.

Supporting Information

Supporting Information is available from the Wiley Online Library or from the author.

Acknowledgements

This research was undertaken on the supercomputers in National Computational Infrastructure (NCI) in Canberra, Australia, which is supported by the Australian Commonwealth Government, and Pawsey Supercomputing Centre in Perth with funding from the Australian government and the Government of Western Australia.

Open access publishing facilitated by Griffith University, as part of the Wiley - Griffith University agreement via the Council of Australian University Librarians.

Conflict of Interest

The authors declare no conflict of interest.

Data Availability Statement

The data that support the findings of this study are available from the corresponding author upon reasonable request.

Keywords

ab initio molecular dynamics, density functional theory, hydrophobicity, nanoscale zero-valent iron, stepped surfaces, sulfidation

Received: March 26, 2023

Revised: May 24, 2023

Published online:

[1] F. He, Z. Li, S. Shi, W. Xu, H. Sheng, Y. Gu, Y. Jiang, B. Xi, *Environ. Sci. Technol.* **2018**, *52*, 8627.

[2] M. Kolos, D. Tunega, F. Karlicky, *Phys. Chem. Chem. Phys.* **2020**, *22*, 23258.

- [3] J. Li, X. Zhang, Y. Sun, L. Liang, B. Pan, W. Zhang, X. Guan, *Environ. Sci. Technol.* **2017**, *51*, 13533.
- [4] J. Xu, Y. Wang, C. Weng, W. Bai, Y. Jiao, R. Kaegi, G. V. Lowry, *Environ. Sci. Technol.* **2019**, *53*, 5936.
- [5] H. Dong, C. Zhang, J. Deng, Z. Jiang, L. Zhang, Y. Cheng, K. Hou, L. Tang, G. Zeng, *Water Res.* **2018**, *135*, 1.
- [6] J. Xu, H. Li, G. V. Lowry, *Acc. Mater. Res.* **2021**, *2*, 420.
- [7] D. Fan, G. O'Brien Johnson, P. G. Tratnyek, R. L. Johnson, *Environ. Sci. Technol.* **2016**, *50*, 9558.
- [8] D. Fan, Y. Lan, P. G. Tratnyek, R. L. Johnson, J. Filip, D. M. O'Carroll, A. Nunez Garcia, A. Agrawal, *Environ. Sci. Technol.* **2017**, *51*, 13070.
- [9] Z. Cao, H. Li, X. Xu, J. Xu, *Chem. Eng. J.* **2020**, *394*, 124876.
- [10] Y. Han, W. Yan, *Environ. Sci. Technol.* **2016**, *50*, 12992.
- [11] Z. Cao, J. Xu, H. Li, T. Ma, L. Lou, G. Henkelman, X. Xu, *Chem. Eng. J.* **2020**, *400*, 125900.
- [12] A. N. Garcia, Y. Zhang, S. Ghoshal, F. He, D. M. O'Carroll, *Environ. Sci. Technol.* **2021**, *55*, 8464.
- [13] Q. Li, Z. Chen, H. Wang, H. Yang, T. Wen, S. Wang, B. Hu, X. Wang, *Sci. Total Environ.* **2021**, *792*, 148546.
- [14] X. Li, L. Zeng, N. Wen, D. Deng, *J. Hazard. Mater.* **2021**, *417*, 126014.
- [15] H. Pang, L. Liu, Z. Bai, R. Chen, H. Tang, Y. Cai, S. Yu, B. Hu, X. Wang, *Sep. Purif. Technol.* **2022**, *285*, 120408.
- [16] Z. Cao, X. Liu, J. Xu, J. Zhang, Y. Yang, J. Zhou, X. Xu, G. V. Lowry, *Environ. Sci. Technol.* **2017**, *51*, 11269.
- [17] J. Xu, A. Avellan, H. Li, X. Liu, V. Noel, Z. Lou, Y. Wang, R. Kaegi, G. Henkelman, G. V. Lowry, *Adv. Mater.* **2020**, *32*, 1906910.
- [18] Q. Bin, B. Lin, K. Zhu, Y. Shen, Y. Man, B. Wang, C. Lai, W. Chen, *J. Environ. Sci.* **2020**, *88*, 90.
- [19] Y. Lü, J. Li, Y. Li, L. Liang, H. Dong, K. Chen, C. Yao, Z. Li, J. Li, X. Guan, *Appl. Catal., B* **2019**, *242*, 9.
- [20] M. Mangayayam, K. Dideriksen, M. Ceccato, D. J. Tobler, *Environ. Sci. Technol.* **2019**, *53*, 4389.
- [21] Z. Cao, H. Li, G. V. Lowry, X. Shi, X. Pan, X. Xu, G. Henkelman, J. Xu, *Environ. Sci. Technol.* **2021**, *55*, 2628.
- [22] J. Chen, H. Dong, R. Tian, R. Li, Q. Xie, *Water Air Soil Pollut.* **2020**, *231*, 432.
- [23] F. He, L. Gong, D. Fan, P. G. Tratnyek, G. V. Lowry, *Environ. Sci. Processes Impacts* **2020**, *22*, 528.
- [24] Y. Mo, J. Xu, L. Zhu, *Environ. Sci. Technol.* **2022**, *56*, 5808.
- [25] J. Xu, Z. Cao, H. Zhou, Z. Lou, Y. Wang, X. Xu, G. V. Lowry, *Environ. Sci. Technol.* **2019**, *53*, 13344.
- [26] C. E. Choong, S. Y. Yoon, K. T. Wong, M. Kim, G. Lee, S.-H. Kim, B.-H. Jeon, J. Choi, Y. Yoon, E. H. Choi, M. Jang, *Chem. Eng. J.* **2023**, *454*, 140083.
- [27] J. J. White, J. J. Hinsch, W. W. Bennett, Y. Wang, *Appl. Surf. Sci.* **2022**, *605*, 154650.
- [28] J. J. White, J. Liu, J. J. Hinsch, Y. Wang, *Phys. Chem. Chem. Phys.* **2021**, *23*, 2649.
- [29] J. J. Hinsch, J. Liu, J. J. White, Y. Wang, *Catalysts* **2022**, *12*, 576.
- [30] G. Kresse, J. Hafner, *Phys. Rev. B: Condens. Matter* **1993**, *47*, 558.
- [31] G. Kresse, J. Furthmüller, *Comput. Mater. Sci.* **1996**, *6*, 15.
- [32] V. X. Wang, N. Xu, J.-C. Liu, G. Tang, W.-T. Geng, *Comput. Phys. Commun.* **2021**, *267*, 108033.
- [33] M. Dion, H. Rydberg, E. Schroder, D. C. Langreth, B. I. Lundqvist, *Phys. Rev. Lett.* **2004**, *92*, 246401.
- [34] T. Thonhauser, V. R. Cooper, S. Li, A. Puzder, P. Hyldgaard, D. C. Langreth, *Phys. Rev. B* **2007**, *76*, 125112.
- [35] J. Klimeš, D. R. Bowler, A. Michaelides, *Phys. Rev. B* **2011**, *83*, 195131.
- [36] K. Lee, É. D. Murray, L. Kong, B. I. Lundqvist, D. C. Langreth, *Phys. Rev. B* **2010**, *82*, 081101.
- [37] G. Kresse, D. Joubert, *Phys. Rev. B* **1999**, *59*, 1758.
- [38] P. Błoński, A. Kiejna, *Surf. Sci.* **2007**, *601*, 123.

- [39] L. Martinez, R. Andrade, E. G. Birgin, J. M. Martinez, *J. Comput. Chem.* **2009**, *30*, 2157.
- [40] M. J. S. Spencer, A. Hung, I. K. Snook, I. Yarovsky, *Surf. Sci.* **2003**, *540*, 420.
- [41] H. Dong, K. Hou, W. Qiao, Y. Cheng, L. Zhang, B. Wang, L. Li, Y. Wang, Q. Ning, G. Zeng, *Chem. Eng. J.* **2019**, *359*, 1046.
- [42] H. Li, W. Yang, C. Wu, J. Xu, *Phys. Chem. Chem. Phys.* **2021**, *23*, 13971.